EARTH SURFACE PROCESSES AND LANDFORMS
Earth Surf. Process. Landforms **40**, 1730–1745 (2015)

Published online 9 June 2015 in Wiley Online Library
(wileyonlinelibrary.com) DOI: 10.1002/esp.3749

Erosion of a high-altitude, low-relief area on the Korean Peninsula: implications for its development processes and evolution

Jongmin Byun,[1]* Arjun M. Heimsath,[2] Yeong Bae Seong[1] and Soo Yong Lee[1]
[1] Department of Geography Education, Korea University, Seoul, Korea
[2] School of Earth and Space Exploration, Arizona State University, Tempe, Arizona

Received 25 November 2013; Revised 23 April 2015; Accepted 23 April 2015

*Correspondence to: Jongmin Byun, School of Civil, Environmental, and Architectural Engineering and BK21 Plus Innovative Leaders for Creating Future Value in Civil Engineering, Korea University, Seoul, Korea. E-mail: cyberzen.byun@gmail.com

ESPL
Earth Surface Processes and Landforms

ABSTRACT: The processes involved in the development of high-altitude, low-relief areas (HLAs) are still poorly understood. Although cosmogenic nuclides have provided insights into the evolution of HLAs interpreted as paleo-surfaces, most studies focus on estimating how slowly they erode and thereby their relative stability. To understand actual development processes of HLAs, we applied several techniques of cosmogenic nuclides in the Daegwanryeong Plateau, a well-known HLA in the Korean Peninsula. Our denudation data from strath terraces, riverine sediments, soils, and tors provide the following conclusions: (1) bedrock incision rate in the plateau (~127 m Myr^{-1}) is controlled by the incision rate of the western part of the Korean Peninsula, and is similar to the catchment-wide denudation rate of the plateau (~93 m Myr^{-1}); (2) the soil production function we observed shows weak depth dependency that may result from highly weathered bedrock coupled with frequent frost action driven by alpine climate; (3) a discrepancy between the soil production and catchment-wide denudation rates implies morphological disequilibrium in the plateau; (4) the tors once regarded as fossil landforms of the Tertiary do not reflect Tertiary processes; and (5) when compared with those of global paleo-surfaces (<20 m Myr^{-1}), our rapid denudation rates suggest that the plateau cannot have maintained its probable initial paleo landscape, and thus is not a paleo-surface. Our data contribute to understanding the surface processes of actively eroding upland landscapes as well as call into question conventional interpretations of supposed paleo-surfaces around the world. Copyright © 2015 John Wiley & Sons, Ltd.

KEYWORDS: cosmogenic nuclides; Daegwanryeong Plateau; peneplain; paleo-surface; soil production; catchment-wide denudation; Korean Peninsula

Introduction

High-altitude, low-relief areas (HLAs) are reported from most of the world's major mountain ranges, including the Pyrenees (de Sitter, 1952), the Rocky Mountains (Epis and Chapin, 1975), the Appalachian Mountains (Meisler, 1962), the Bolivian Andes (Kennan *et al.*, 1997), the Deccan Plateau (Gunnell, 1998), the Himalaya (van der Beek *et al.*, 2009), the Gobi Altai (Jolivet *et al.*, 2007), ranges in Australia (Twidale and Campbell, 1995), Japan (Sugai and Ohmori, 1999), Korea (Kim, 1973), and Papua New Guinea (Abbott *et al.*, 1997).

These HLAs are interpreted as uplifted paleo-surfaces (i.e. erosional surfaces formed initially at sea level and then uplifted), which have not yet adjusted to contemporary uplift and correspondent stream incision. Since they act as passive markers to vertical motion of the Earth's surface, their modern altitude provides a useful datum for measuring surface uplift and the magnitude of river incision (Clark *et al.*, 2005). They are, therefore, considered to be important for understanding the timing and magnitude of orogenesis, and post-orogenic landscape evolution. Furthermore, such surfaces remain in the midst of the debate between the late Cenozoic uplift of modern mountain belts through the world and global climate change (Molnar and England, 1990).

Interpretation of HLAs as uplifted paleo-surfaces has, however, generated considerable debate on the origin of HLAs, because such an interpretation would require a very long stable period followed by significant, rapid, and recent uplift (Gunnell *et al.*, 2009). Moreover, recent studies have argued that the relief of mountain belts could be reduced at high elevation (Babault *et al.*, 2005), and that HLAs might have formed recently by interactions between local lithology and contemporary surface processes (Anderson, 2002). Such alternative explanations for the HLA formation would not necessarily require a complicated landscape evolution history invoking an erosional surface formed at a paleo sea level and then uplifted.

A complete solution to address this controversy requires quantification of modern surface processes shaping HLAs. Recent advances in accelerated mass spectrometry enable us to quantify geomorphic processes with terrestrial cosmogenic nuclides (Lal, 1991; Gosse and Phillips, 2001; Dunai, 2010; Granger *et al.*, 2013). Since the concentration of cosmogenic nuclides measured in a surface material reflects the history of exposure of this material, it is possible to estimate the exposure

ages and denudation rates of exposed rocks (Lal, 1991), catchment-wide denudation rates from fluvial sediments (Bierman and Steig, 1996), and soil production rates that can indicate the upper limit of local steady-state erosion rates across soil-mantled landscapes (Heimsath *et al.*, 1997). Such efforts to quantify the rates of surface processes have led to a better understanding of landscape evolution in many regions.

Within the various geomorphic applications of cosmogenic nuclides, there have been a handful of studies examining the evolution of HLAs (Small *et al.*, 1997; Belton *et al.*, 2004; Hancock and Kirwan, 2007; Vanacker *et al.*, 2007; Strobl *et al.*, 2012; Walcek and Hoke, 2012). These previous studies yielded denudation data rather than simple qualitative assessments. Thus, more explicit explanations, either supporting stability during the evolution of HLAs (Hancock and Kirwan, 2007; Strobl *et al.*, 2012; Walcek and Hoke, 2012) or denying longevity of HLAs (Belton *et al.*, 2004), became possible. Such research efforts focused, however, on yielding representative denudation rate or exposure age of the landscape in each HLA to estimate how slowly it is eroding or test whether its evolution over geologic time scales has been stable or not. Moreover, quantitative data from these studies are mostly from the bedrock features such as exposed bedrock outcrops that provide only a lower bound on denudation rates (Portenga and Bierman, 2011). Previously collected data do not, therefore, enable a complete picture of the evolution of HLAs to be established.

In this respect, the combination of rates across soil production (indicating ground surface lowering rate), catchment-wide denudation, river incision, and bedrock denudation can provide a more complete approach to understand actual development processes of HLA. To this end, we apply several techniques of

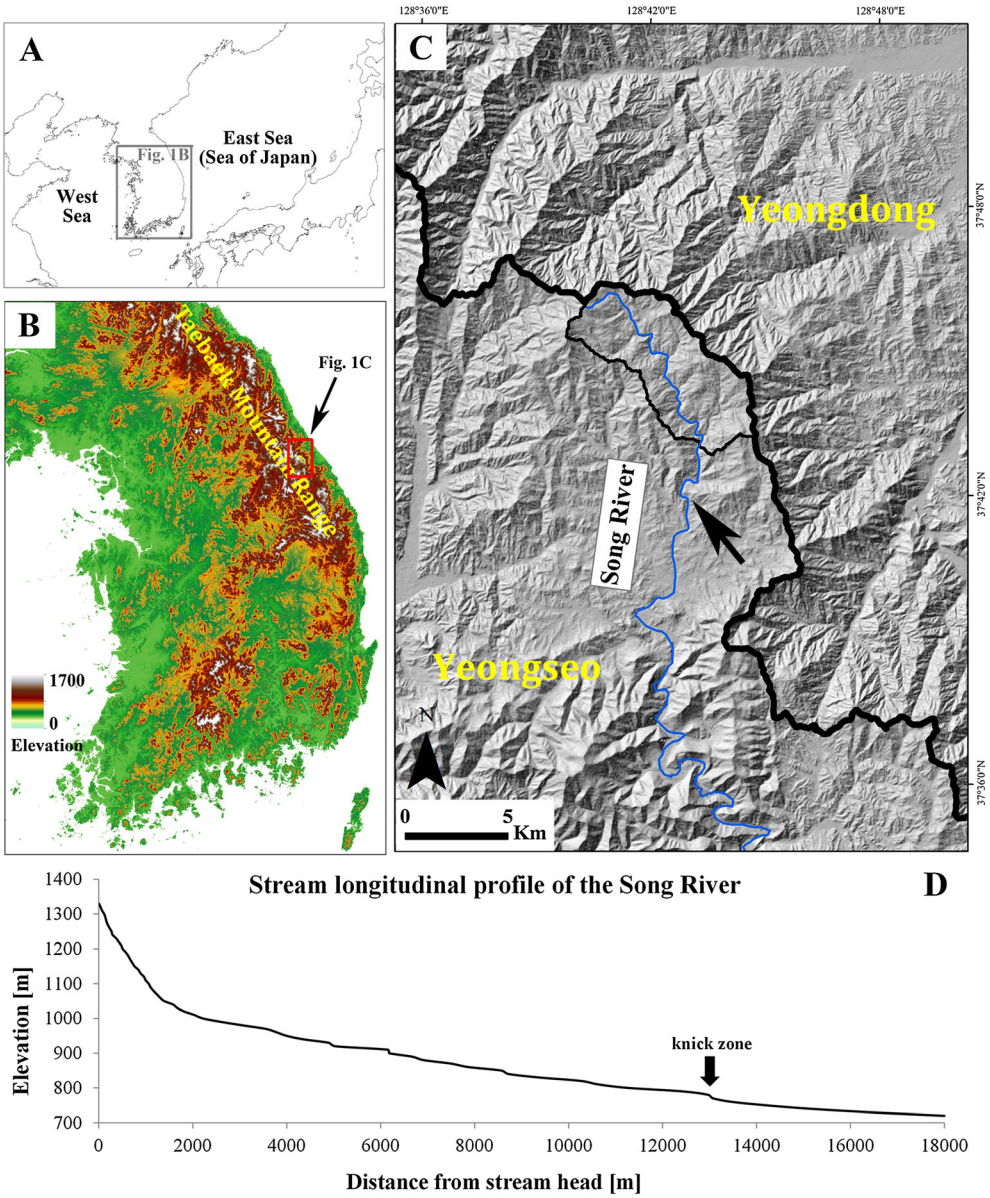

Figure 1. Location of the study area. (A) Map of the Korean Peninsula. (B) The group of high mountains with a NNE–SSE trend is the Taebaek Mountain Range, on which the study area is located. (C) The study area, featuring a low-relief, hilly landscape, is delineated by the thin black line. Thick black line is the ridge line of the Taebaek Mountain Range that separates the west side of the peninsula of which elevation becomes gradually lower as it goes to the west (Yeongseo) with the east side of the peninsula including steep, dissected landscapes draining through the east coastal plain of the peninsula to the East Sea (Yeongdong). The Song River running through the study area flows through the Yeongseo area finally to the West Sea. The north and east border of the study area is confronting the Yeongdong Area with a steep landscape. The arrow indicates the location of a knick zone that separates morphologically the study area from the down-stream area. (D) The longitudinal profile of the Song River and a knick zone. The profile was generated using a 1:25,000-scale contour topographic map of the area. This figure is available in colour online at wileyonlinelibrary.com/journal/espl

cosmogenic radionuclides to the Daegwanryeong Plateau, a well-known HLA in the Korean Peninsula, characterized as a soil-mantled hilly landscape. To be specific, we quantify bedrock incision rates, catchment-wide denudation rates, soil production rates, and denudation rates of tors, and then analyze these data using comparative analysis with topographic indices of the study area to determine the key geomorphic processes in the plateau and evaluate long-term landscape evolution of a typical HLA.

Research Area

The study area of the Daegwanryeong Plateau is located at the top of the Taebaek Mountain Range, which extends along the eastern margin of the Korean Peninsula, forming its backbone (Figure 1(A), (B)). The topography of the middle part of the peninsula is characterized by lower elevations to the west and higher terrain to the east including the Taebaek Mountain Range. The contrasting topographic pattern across the middle part of the peninsula is assumed to have originated from the tilted tectonic up-warping in the mid-Miocene (Kim, 1973), which is related to processes associated with the opening of the East Sea (or Sea of Japan) (Park and Kim, 1971; Kim, 1992).

Some recent pioneering efforts to quantitatively assess the building of the Taebaek Mountain Range, on which the Daegwanryeong Plateau is located, yielded long-term exhumation rates using apatite fission track (Han, 2002) and single-grain (U-Th)/He dating (Min *et al.*, 2008, 2010) on granitic rocks along a vertical transect in the Daegwanryeong area, and inferred an uplift history using a numerical landscape evolution model (Byun, 2011). According to the fission track data, the study area had been exhumed slowly at a rate of ~62 m Myr^{-1} from the mid Eocene (47 Ma) to the late Oligocene (23 Ma) (Han, 2002). After the slow exhumation period, however, the (U-Th)/He data shows elevation independent ages below 600 m of the transect indicating a pulse of rapid exhumation at 22 ± 3 Ma ago, which is coeval with the opening of the East Sea (Min *et al.*, 2010). Therefore, Min *et al.* (2010) suggested that the rapid building mechanism of the Taebaek Mountain Range is intimately interconnected with the opening of the East Sea. Since the rapid exhumation, the uplift rate of the study area has decreased exponentially (Byun, 2011).

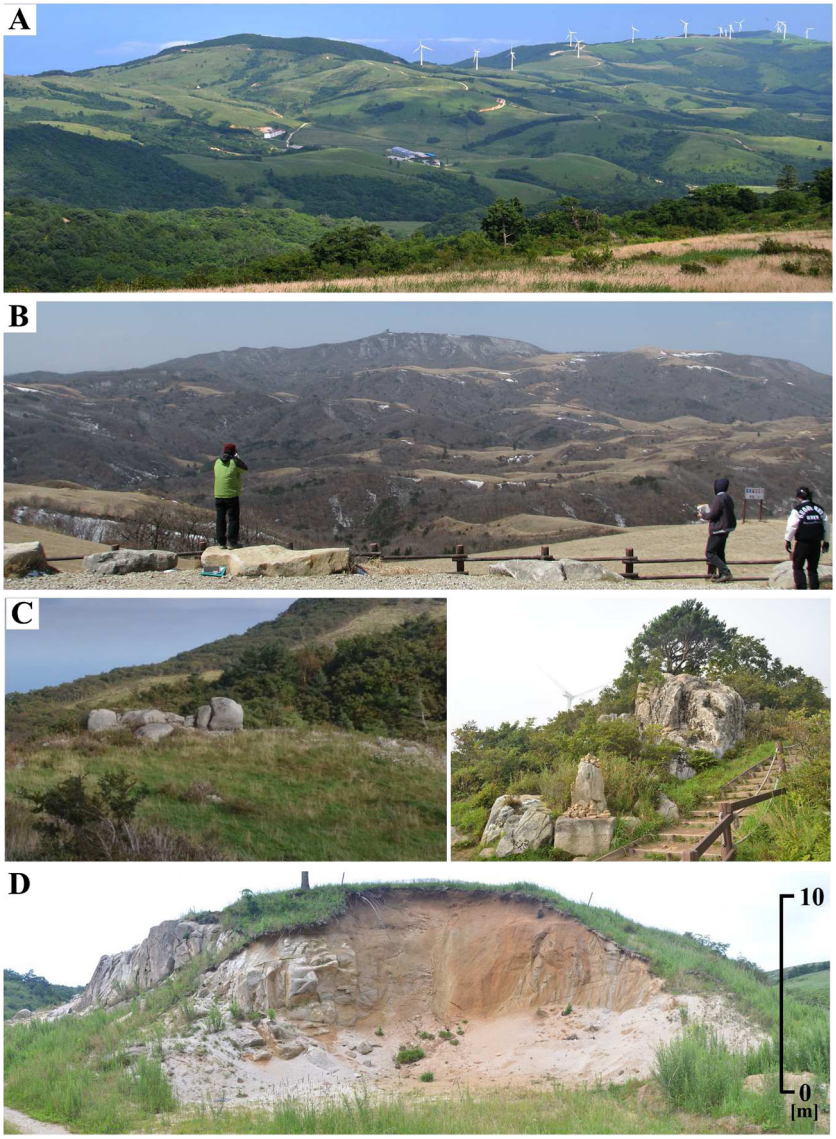

Figure 2. Photo composite of the study area. The Daegwanryeong Plateau features a low-relief, hilly landscape (A), (B) that features convex slopes and wide, flat hilltops. This landscape has been interpreted by many authors as the remnants of a paleo-surface formed before the uplift of the Korean Peninsula. Tors are another landscape element of the study area (C). They are sparsely distributed along the ridges of soil-mantled hillslopes, and their flat and angular shapes are controlled mainly by joints. The underlying bedrock is granite, most of which is highly weathered (D). This figure is available in colour online at wileyonlinelibrary.com/journal/espl

In addition to the Daegwanryeong Plateau, many other HLAs occur on the tops of the major mountain ranges of the Korean Peninsula. Since the 1930s, these features have been thought to be uplifted paleo-surfaces, such as peneplains or etch plains, which had formed at a paleo sea level before uplifting of the major mountain ranges of the peninsula (Kobayashi, 1931; Kim, 1980). The Daegwanryeong Plateau is regarded as the best example of such paleo-surfaces, because it is the most extensive in area (Figures 1(C) and 2(A), (B)). However, the interpretation of the Daegwanryeong Plateau as a paleo-surface is also an issue under recent debate. A recent notable study (Park, 2009), although its basis was established only from topography analysis, suggested that forming processes of the Daegwanryeong Plateau are dependent on its geological characteristics and historical contingency during landform development.

Elevations of the study area range from ~830 to ~1400 m, and thus the study area is characterized by a typical alpine climate: low temperatures, orographic precipitation, and strong winds (Supplementary Figure 1). Weathering and erosional processes in the study area are controlled primarily by frequent frost actions due to repetitive freeze–thaw cycles during the longer winter season, but erosion by overland flow due to severe rainfall events during the summer monsoon is relatively minor because of vegetation cover during the summer monsoon (Kee, 2002). Because of few frost-free days (<150 days per year) due to the longest winter season in South Korea (Kwon, 2006) but also difficulty in settlement due to inaccessibility from nearby urban areas, land use at the study area has long been very limited (Editorial board for Samyang Food's thirty year history's, 1991). Since 1972, however, natural forests of the Daegwanryeong Plateau, especially on the wide, flat hill tops, were cleared and replaced with herbage plants for raising cows (Editorial board for Samyang Food's thirty year history's, 1991). Although soil loss due to the change of land cover may have increased, the increased amounts may not be as severe as those in the areas under active cultivation (Park *et al.*, 2010) because strong coupling of the roots of the herbage plants has prevented soil loss from erosion by overland flow during the summer monsoon (Editorial board for Samyang Food's thirty year history's, 1991; Kee, 2002).

The study area is dominated by soil mantled hillslopes with convex slopes and wide, flat hilltops (Supplementary figure 2). Tors are distributed sparsely along the ridges (Figure 2(C)). The underlying lithology of the study area is granite intruded during the Jurassic (Kim *et al.*, 2001). Highly weathered saprolites can be 10 m thick and are typically overlain by shallow (<1 m thick) soils (Figure 2(D)). These deep weathered saprolites are assumed to be products of deep weathering under the warmer, humid climate that prevailed during the Tertiary (Kim, 1980). However, a recent study (Kee, 2002) based on microscope observations of cracked minerals in the saprolite and the soil Bt horizon, suggested that frequent frost action under the periglacial climate shattered minerals in the saprolites and may lead to increased chemical weathering of granite.

Methods

Cosmogenic nuclides

To establish a comprehensive understanding of the landscape evolution of the Daegwanryeong Plateau we measured ^{10}Be concentrations in the surface and near-surface materials of the plateau to determine soil production rates on soil-mantled hillslopes, exposure ages and denudation rates of tors on the ridges of hillslopes, catchment-wide denudation rates of subcatchments, as well as exposure ages of strath terraces that enable one to infer river incision rates.

For a bedrock surface that is assumed to be eroding at a nearly constant rate by grain–grain spallation or exfoliation in thin sheets, the denudation rates and exposure ages of these exposed bedrock surfaces can also be calculated from the nuclide concentrations of the exposed surfaces (Lal, 1988). In particular, nuclide concentration data for a series of samples taken

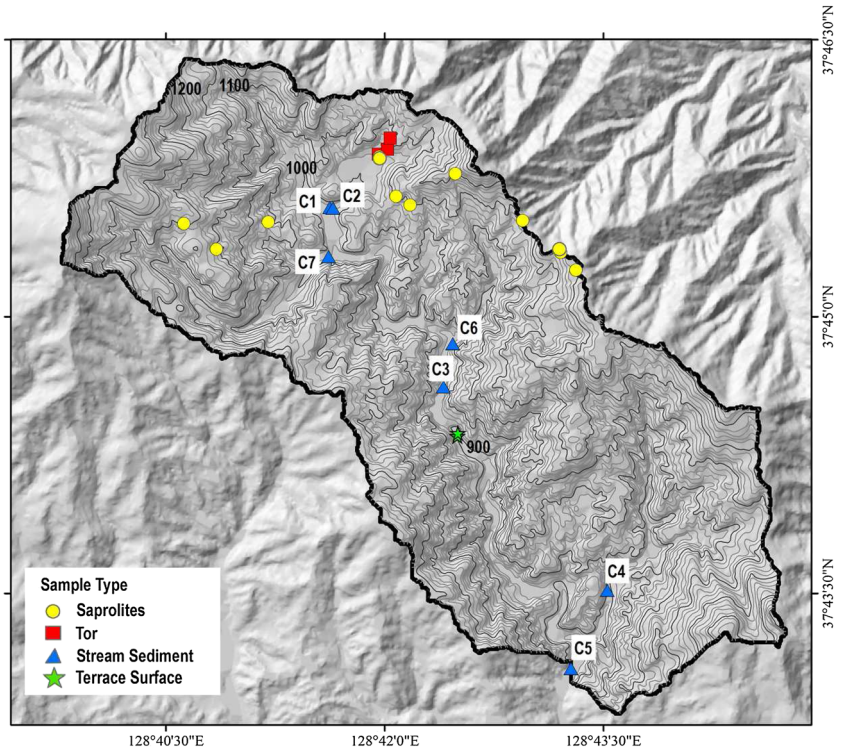

Figure 3. Sampling sites on a contour topographic map. Most sampling sites are concentrated in the northern part of the study area, which shows a well-developed low-relief, hilly landscape. This figure is available in colour online at wileyonlinelibrary.com/journal/espl

from top to bottom of a tor profile should give insight into tor emergence and evolution (Heimsath *et al.*, 2000, 2001a, 2001b). Catchment-wide denudation rates can also be calculated from the nuclide concentrations of fluvial sediment (Brown *et al.*, 1995; Bierman and Steig, 1996; Granger *et al.*, 1996) in a similar way to the calculation of bedrock denudation rate. When calculating catchment-wide denudation rates, however, we use the ^{10}Be production rate averaged over elevations and latitudinal variations within the catchment (Portenga and Bierman, 2011).

If the bedrock (or weathered bedrock) conversion rate to soil (i.e. soil production rate) is the same as the surface lowering rate due to downslope transportation of soil and thus soil thickness is in local steady state, then the rate of soil production can be calculated from the nuclide concentration at the soil–bedrock interface (Heimsath *et al.*, 1997). Deeply weathered saprolites are extensive on the Daegwanryeong Plateau. We focus on the underlying saprolites that have not been physically mobilized and thereby retain relict rock structure as weathered bedrock. Conversely, we define the physically mobile layer that has been perturbed by living organisms and is undergoing downslope transport as soil. Such division of weathering profile was formally presented in Yoo and Mudd (2008).

Sampling strategy

In total, 27 samples were collected across the study area: 13 samples for examining soil production rate, five for tor exposure age and denudation rate, seven for catchment-wide denudation rate, and two for bedrock incision rate (Figure 3). Most sampling sites are located in the northern portion of the Daegwanryeong Plateau. This area is largely dominated by low-relief, hilly landscape with convex slopes and wide, flat hilltops and thus representative of the whole plateau. Because the Korean National Park Service has protected the area for several decades, it has remained relatively free of recent human activities. Therefore, we consider that our results should reliably reflect the natural erosion processes of the Daegwanryeong Plateau.

Two samples were collected from the surfaces of strath terraces with different elevations (Figure 4(A), (B)). The height of each terrace surface above the current river was measured using a total station. The exposure ages of these terrace surfaces, when combined with their height above the modern river, can provide estimates of the average rate of bedrock incision. To infer catchment-wide denudation rates of sub-catchments, fluvial sand samples were collected from the surface of active sand bars deposited by current stream channels. These samples seem to be representative of the sediments exported from each sub-catchment, because most areas of the Daegwanryeong Plateau are covered with sand–silt-sized soils and saprolites (Kee, 2002). We collected five samples (C1, C2, C4, C6, and C7) from the upstream part of each junction between the main stream and tributary, and two samples (C3 and C5) from points along the main stream (Figure 3).

Samples for determining soil production rates were collected from the top of the saprolites across the convex-up ridges of hillslopes, where soil creep dominates (Figures 3 and 4(C)). Convex hillslope ridges are most likely to be experiencing steady-state erosional processes such that local soil thicknesses have been roughly constant for the effective irradiation time (Lal, 1991) for the *in situ* cosmogenic nuclides at the top of saprolites to attain the secular equilibrium concentration. The soil thickness measured at each location was corrected to slope-normal soil thickness by using local slope and we measured bulk density of the saprolite and overlying soils at each sampling site with a corer (Figure 4(E)).

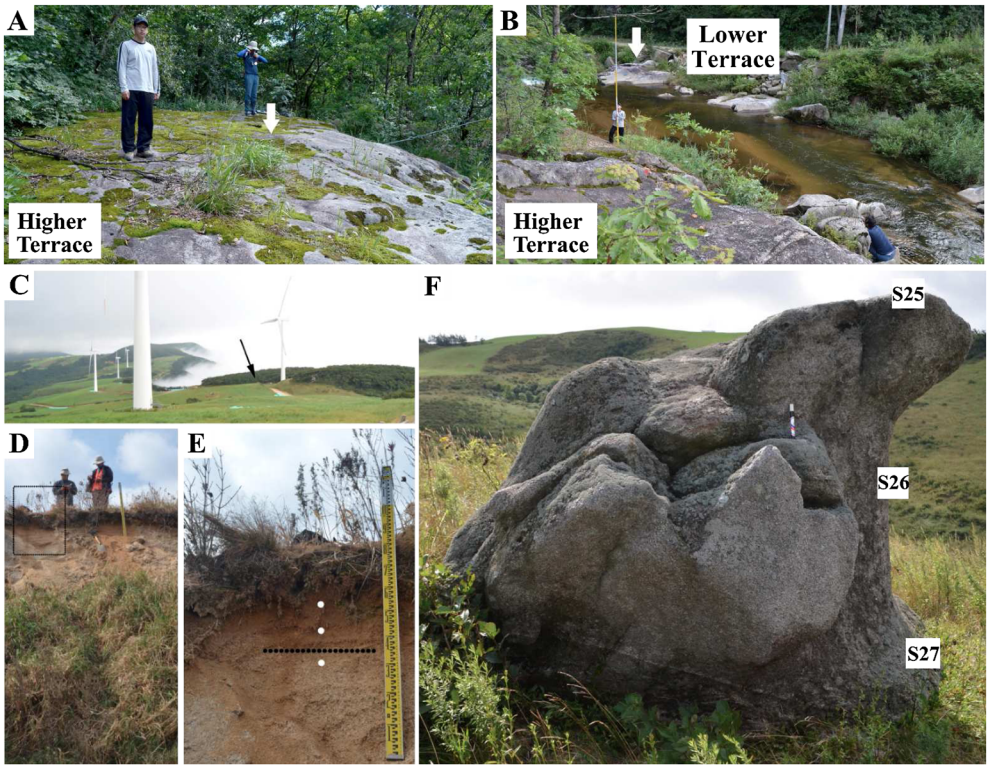

Figure 4. Photo composite for sampling sites. Sampling sites for bedrock incision rates (A), (B), soil production rates (C, D, E), and tor exposure ages (F). The white arrows in (A) and (B) indicate sampling points on the strath terraces (B0 and B3 in Table II). The relative heights of these terraces above the current channel are 0.96 and 3.98 m, respectively. The horizontal extents of the higher and lower terrace are about 8 and 2 m at least, respectively. Both terraces have direct evidences for bedrock incision such as carved potholes. The distance between both sampling sites is about 25 m at least. (C) A sampling site for soil production rate on the convex-up ridge of hillslope (black arrow in (C)). The black inset box in (D) indicates the section covered by (E) that shows the interface (black dotted line) between soil and saprolite. White dots in (E) are points for measurement of bulk density. This figure is available in colour online at wileyonlinelibrary.com/journal/espl

For examining tor exposure and evolution, we collected five samples from tor surfaces: three from a vertical profile of one tor (S25, S26, S27) and one each from the tops of two other tors (S13, S28). Three profile samples were taken from the tallest tor in the study area, at sample heights of 0.2, 1.1, and 2 m above the ground surface (Figure 4(F)). Unlike the tallest tor from which the profile samples were taken, the heights of the other two tors are ~1.6 m and near-ground level (~0.3 m). Therefore denudation rate from the two lower tors can be used to compare with soil production rates that are indicative of near-ground soil lowering rate as well as those from the profile samples of the tallest tor to understand tor emergence and development in the study area. We also measured the Schmidt hammer rebound value of each sampling point to assess the weathering status of the point (Goudie, 2006).

Sample preparation and ^{10}Be concentration measurement

The physical and chemical procedures for ^{10}Be measurements were performed in the Geochronology Laboratory at Korea University, Korea. Bedrock, saprolite, and fluvial sediments from samples were crushed, sieved to the 250–500 μm size fraction, and chemically purified following the conventional procedures described by Kohl and Nishiizumi (1992) to yield quartz from which Be was extracted. After the addition of a low-background ^{9}Be carrier, Be was separated and purified by ion-exchange chromatography and precipitated at pH > 7. Hydroxides were oxidized by ignition in quartz crucibles. BeO was mixed with Nb metal and loaded onto targets to measure the ^{10}Be/^{9}Be ratio by AMS at the Korea Institute of Geology and Mineralogy, Daejeon, Korea. The measured Be isotope ratios were compared with ^{10}Be standards (ICN Pharmaceuticals) prepared by Nishiizumi *et al.* (2007) and using a ^{10}Be half-life of 1.36×10^{6} year (Chmeleff *et al.*, 2010; Korschinek *et al.*, 2010). The measured isotope ratios were converted to cosmogenic ^{10}Be concentrations in quartz using the total ^{10}Be in the samples and the sample weights.

Topographic and climatic indices

To analyze which topographic properties are related to the measured catchment-wide denudation rates, we derived topographic indices (slope, curvature, and relief) from a 25 m gridded DEM based on ASTER GDEM V2 using ArcGIS. Moreover, frequent frost actions during the long winter season are also regarded as a dominant process in the study area (Kee, 1999) and we calculated mean elevation values of every sub-catchment as a simple variable to explain the degree of frost action. Soils and rocks become more exposed to frost actions with altitude as temperature decreases with altitude (Kitayama, 1992). However, the amount of rainfall also increases with altitude (Smith, 1979), and we also calculated annual precipitation values of every sub-catchment in the study area based on the digital climate model provided by the National Center for Agro Meteorology (http://www.ncam.kr). The precipitation data are useful to separate the effects of the orographic precipitation from those of the decreased temperature with altitude. Finally, we correlated the above topographic and climatic indices with our denudation data.

Results

The exposure ages of the higher and lower strath terraces are 31.2 ± 7.3 and 14.6 ± 5.0 Ka, respectively (Table I). Using these exposure ages and their relative heights beyond the modern stream level (3.98, 0.96 m), we calculate a long-term average bedrock incision rate and two sub-bedrock incision rates since the abandonment of the higher terrace (Supplementary Figure 3). The averaged incision rate calculated from the relative height of the higher terrace and its exposure age is 127.7 ± 27.4 m Myr^{-1}. The first sub-bedrock incision rate during the period between the abandonment of the higher terrace and the formation of the lower terrace was 187 m Myr^{-1}, and the second sub-incision rate since the abandonment of the lower terrace was 67 m Myr^{-1}.

Catchment-wide denudation rates from low-order, small sub-catchments (C1, C2, C3, C4, C6, and C7) range from 52 to 119 m Myr^{-1} (Table II and Figure 5(A)). Their mean value (93 ± 22 m Myr^{-1}) is close to the denudation rate of the largest catchment C5 containing all of the above sub-catchments (102 ± 23 m Myr^{-1}). According to the correlation analysis to determine which surface processes best explains the variance in these denudation rates, there are positive but weak correlations with elevation ($P = 0.54$), precipitation ($P = 0.50$), slope ($P = 0.45$) and relief ($P = 0.43$), and no correlations with curvature ($P = 0.20$) and upstream area ($P = 0.25$) (Figure 6).

The soil production rates tend to decrease with increasing soil depth (Figure 7; Table I). Following Heimsath *et al.* (1997 and subsequent studies) we determined a soil production function from a variance-weighted least-squares best fit model of the relationship between soil production rate and soil depth (Figure 7) as:

$$\varepsilon = (54 \pm 1) e^{(-0.0068 \pm 0.0026)h} \quad (1)$$

where ε is soil production rate (m Myr^{-1}) and h is slope-normal soil depth (cm).

The ^{10}Be concentrations of samples from a tor profile (S25, S26, S27) show little variation with height (Table I and Figure 8). Moreover the apparent exposure ages at the middle and bottom sampling points (S26, S27) are very similar. These results suggest the possibility that the ground surface around the tor lowered rapidly after the tor had been exposed (Heimsath *et al.*, 2001a, 2001b). However, additional calculated data and field observations from the tor do not support this notion. This will be considered in more detail in the discussion section.

Discussion

Controls on bedrock incision

The average bedrock incision rate is 127.7 ± 27.4 m Myr^{-1}, calculated using only the higher terrace (Finnegan *et al.*, 2014). Coincidentally, this value overlaps the lowering rates of the westerly drainages of the study area (150 ~ 205 m Myr^{-1}) that are determined based on the chronology of fluvial terraces from optically stimulated luminescence dating (Yoon *et al.*, 2007; Lee, 2009). Given that the bedrock incision rate of the study area is close to the regional incision rate of the western part of the Korean Peninsula, this implies that the base-level lowering rate in the Daegwanryeong Plateau is likely to have been controlled by the regional tectonics of the western part of the Korean Peninsula.

However, the base-level in the study area may have been lowered not constantly but intermittently (from ~190 to ~70 m Myr^{-1}). Such a sudden change in bedrock incision rate may have been driven by the migration of a knickpoint that is located immediate upstream of the strath terrace where we sampled (B0 and B3). Although the height of the knickpoint is

Table I. Soil production rates, denudation rates and exposure ages of tors and strath terraces in the Daegwanryeong Plateau study area

Sample	Latitude	Longitude	Elevation[a]	Depth[b]	Slope	Density[c]	Shielding factor	Production rate by spallation[d]	^{10}Be conc[e]	+/−[f]	E[g]	+/−[h]	Age[i]	+/−[j]	Time scale[k]
	[°N]	[°E]	[m]	[cm]	[°]	[g cm^{-3}]		[atoms g^{-1} yr^{-1}]	[atoms g^{-1}]		[m Myr^{-1}]		[yrs]		[Ka]
Weathered bedrock															
S1	37.7542	128.7219	1110	39	10	1.30	0.9998	7.50	266794	35390	34.0	5.7	-	-	36.2
S2	37.7558	128.7201	1096	53	14	1.36	0.9983	6.65	236620	19417	32.5	4.3	-	-	36.2
S3	37.7558	128.7201	1096	19	14	1.20	0.9983	8.65	297278	26044	38.1	5.0	-	-	35.0
S4	37.7629	128.7081	1117	62	22	1.25	0.9948	6.29	132339	21140	60.2	12.1	-	-	21.3
S5	37.7561	128.6808	1161	68	25	1.62	0.9982	6.25	211395	27482	28.7	4.1	-	-	34.4
S1-2	37.7542	128.7219	1110	9	10	1.02	0.9998	9.50	213570	25301	69.0	11.1	-	-	22.7
S11	37.7587	128.7158	1040	4	5	0.80	0.9999	9.35	312945	28952	58.7	9.4	-	-	34.1
S12	37.7647	128.6993	1020	14	20	1.27	0.9918	8.44	232123	26167	45.2	6.5	-	-	27.9
S14	37.7601	128.7029	1040	24	10	1.30	0.9985	8.02	148875	23020	65.7	11.8	-	-	18.7
S21	37.7609	128.7013	1052	91	12	1.72	0.9954	4.79	139941	17783	31.4	4.2	-	-	29.7
S23	37.7584	128.6770	1212	46	2	1.40	0.9997	7.71	170233	17110	51.2	7.0	-	-	22.3
S24°	37.7585	128.6867	1074	35	20	0.80	0.9936	7.52	63738	21404	233.6	94.4	-	-	8.5
S29°	37.7645	128.6994	1028	11	22	1.09	0.9720	8.52	64474	24593	193.2	77.2	-	-	36.2
Tor															
S13	37.7647	128.6993	1020	2	0	2.65	0.9974	9.47	212160	24278	26.6	3.4	22530	2610	22.7
S25[l]	37.7652	128.7004	1031.0	2	0	2.65	0.9993	9.57	121755	48273	47.2	19.0	12758	2077	12.8
S26[l]	37.7652	128.7004	1030.1	2	90	2.65	0.4454	4.27	81595	42192	31.3	16.4	19215	9987	19.3
S27[l]	37.7652	128.7004	1029.2	2	90	2.65	0.5008	4.80	89279	20784	32.1	7.7	18696	4380	18.8
S28	37.7661	128.7006	1053	2	0	2.65	0.9993	9.74	395208	43927	14.6	1.8	40993	4636	41.4
Strath Terrace															
B0[m]	37.7392	128.7083	911 (0.96)	2	0	2.65	0.9543	8.18	119019	40673	-	-	14603	5013	-
B3[m]	37.7395	128.7084	914 (3.98)	2	0	2.65	0.9699	8.39	259558	60064	-	-	31178	7283	-

[a]Value in brackets is relative height of a sampling point above the current channel.
[b]Depth for soil sample is soil thickness and was corrected by local slope. Depth for tor is thickness.
[c]Density for saprolite is bulk density of soil above the interface between soil and saprolite (or weathered bedrock) and was used for calculating soil production rate.
[d]Constant (time-invariant) local production rate based on Lal (1991) and Stone (2000). A value for sea level at high latitude (4.49 atoms ^{10}Be g^{-1}) based on the Cosmic-Ray Produced Nuclide Systematics (CRONUS) Earth online calculator version 2.2.1 (hppt://hess.ess.washingonledu/) was used.
[e]Blank corrected ^{10}Be concentration. ^{10}Be/^{9}Be ratio was measured by AMS at the Korea Institute of Geology and Mineralogy, Daejeon, Korea. Isotope ratio measured were normalized to KN Standard Be 0152 prepared by Nishiizumi *et al.* (2007) with ^{10}Be/^{9}Be ratio of 8.558×10^{-12} and using a ^{10}Be half-life of 1.36×10^{6} years (Chmeleff *et al.*, 2010; Korschinek *et al.*, 2010).
[f]Propagated uncertainty of ^{10}Be concentration includes errors from the blank and AMS
[g]E for saprolite is soil production rate and was calculated using local soil density measured at each sampling site. E for tor is denudation rate of tor.
[h]Propagated error of soil production rate includes errors from soil depth, soil density and ^{10}Be concentration.
[i]Exposure ages for tors and strath terraces were calculated without consideration of muons effect.
[j]Propagated error in exposure ages include a 6% uncertainty in the production rate of ^{10}Be and a 4% uncertainty in the ^{10}Be decay constant.
[k]The time over which the soil production and denudation rate integrate is calculated by dividing the absorption length scale (~1.3 m for soil production and ~60 cm for tor denudation respectively) by the denudation rate.
[l]Samples vertically taken from a tor profile. S25 was taken at the top horizontal surface, S26 at the middle vertical surface, S7 at the bottom vertical surface. Their relative heights above the ground surface are 2, 1.1, and 0.2 m respectively.
[m]Samples for calculating bedrock incision rate around the Daegwanryeong Plateau. B0 and B3 were taken from the lower and higher terrace surface respectively.
[n]Two samples (S24 and S29) yield rates that are at least four times higher than rates of adjacent samples with similar depths. We disregard both samples when plotting the soil production function because they have error ~40 %, which are likely due to error of AMS measurements at that time.

Table II. Catchment-wide denudation rates yielded from *in situ* ^{10}Be concentrations of the Daegwanryeong Plateau stream sediments and topographic indices of subcatchments

Symbol	Latitude [°N]	Longitude [°E]	Elevation of sample [m]	Mean catchment elevation [m]	Mean topographic shielding factor[a]	Mean production rate by spallation[a] [atoms g^{-1} yr^{-1}]	^{10}Be conc[c] [atoms g^{-1}]	+/−[d]	E[e] [m Myr^{-1}]	+/−[f]	Time scale[g] [Ka]	Slope [°]	Upstream area [km^2]	Mean curvature	Local relief [m]
Stream sediment[h]															
C1	37.75984	128.69374	995	1141	0.9941	10.97	91815	19886	119.0	31.4	8.4	13.8	2.8	−0.0028	57.9
C2	37.75979	128.69410	997	1053	0.9968	10.24	98239	12323	103.8	19.1	9.6	11.6	1.4	0.0027	46.6
C3	37.74367	128.70675	933	1082	0.9945	10.47	145268	15014	71.6	13.1	14.0	13.1	11.7	−0.0027	53.8
C4	37.72526	128.72550	866	996	0.9951	9.77	100505	15676	96.7	20.5	10.3	13.0	4.6	−0.0016	54.5
C5	37.71818	128.72132	837	1033	0.9942	10.07	98573	15784	101.6	22.6	9.8	13.5	22.7	−0.0006	55.8
C6	37.74753	128.70779	936	1035	0.9946	10.07	193744	22861	51.5	9.4	19.4	12.3	1.9	−0.0016	50.7
C7	37.75542	128.69359	997	1147	0.9933	11.01	104040	30651	105.3	34.9	9.5	14.2	2.9	0.0033	59.0

[a]We calculated shielding factor and production rate by spallation for each catchment using the 10 m DEM made from the topographic digital map provided by the National Geographic Information Institute of Korea and the MATLAB script initially prepared by Greg Balco (http://depts.washington.edu) which were modified properly for our purpose.

[b]Constant (time-invariant) local production rate based on Lal (1991) and Stone (2000). A value for sea level at high latitude (4.49 atoms ^{10}Be g^{-1}) based on the CRONUS Earth online calculator version 2.2.1 (hppt://hess.ess.washingonledu/) was used.

[c]Blank-corrected ^{10}Be concentrations. ^{10}Be/^{9}Be ratio was measured by AMS at the Korea Institute of Geology and Mineralogy, Daejeon, Korea. Isotope ratio measured was calibrated using KN Standard Be 0152 with a ^{10}Be/^{9}Be ratio of 8.558×10^{-12} (cf. Nishiizumi *et al.*, 2007) and using a ^{10}Be half-life of 1.36×10^{6} years (Chmeleff *et al.*, 2010; Korschinek *et al.*, 2010).

[d]Propagated uncertainty of ^{10}Be concentration includes errors from the blank and AMS.

[e]Catchment-wide denudation rate. When calculating, the bulk density of steadily eroded material was considered as 1.6 g cm^{-3} because the most region of the study area is underlain by deep weathered saprolites.

[f]Propagated error includes errors from saprolite density and ^{10}Be concentration.

[g]The time over which the denudation rate integrates is calculated by dividing the absorption length scale of ~1 m by the denudation rate.

[h]For determining catchment-wide denudation rates from stream sediment samples, we used the 0.25–0.5 mm grain size fraction.

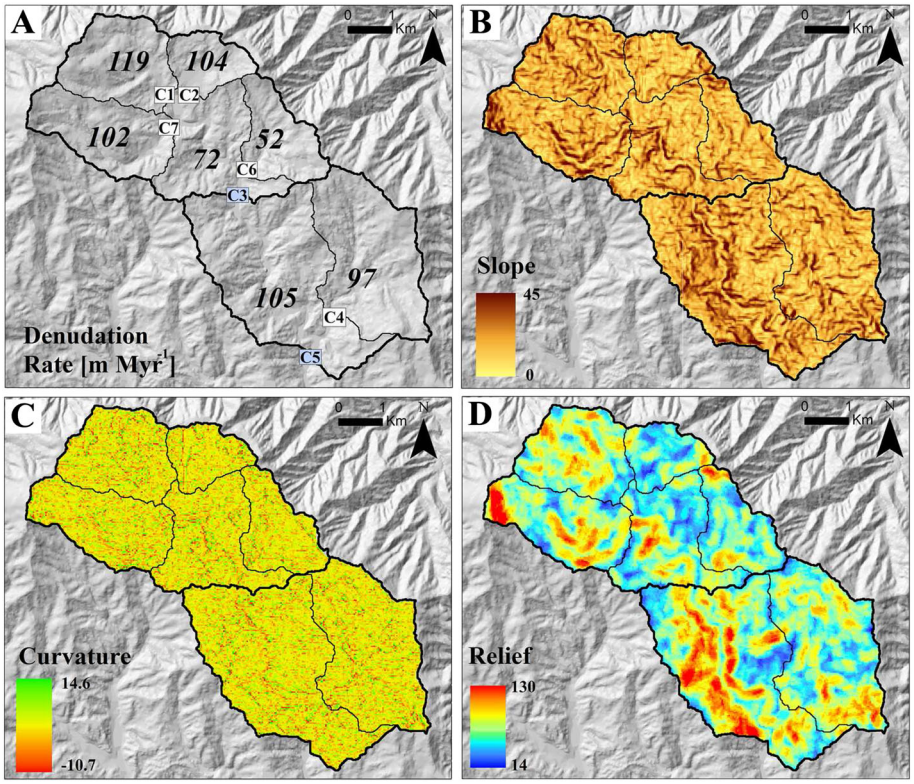

Figure 5. Catchment-wide denudation rates and topographic indices of the Daegwanryeong Plateau. (A) Catchment-wide denudation rates. (B) Slope (degrees). (C) Mean curvature (m^{-1}). (D) Local relief. The topographic indices were calculated using a 25 m gridded DEM based on the ASTER GDEM V2. This figure is available in colour online at wileyonlinelibrary.com/journal/espl

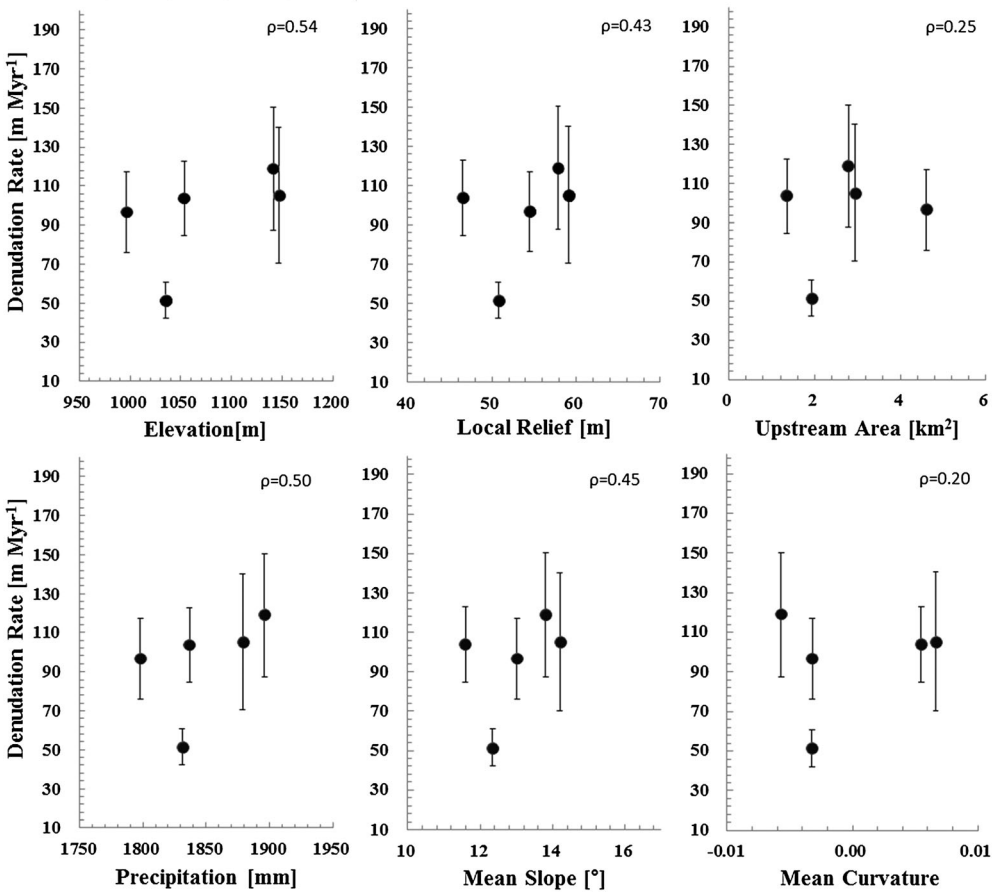

Figure 6. Catchment-wide denudation rate versus topographic indices (elevation, relief, slope, upstream area, curvature) and precipitation. ρ in the figure is correlation coefficient. Different error bars come from saprolite density and ^{10}Be concentration (Table II).

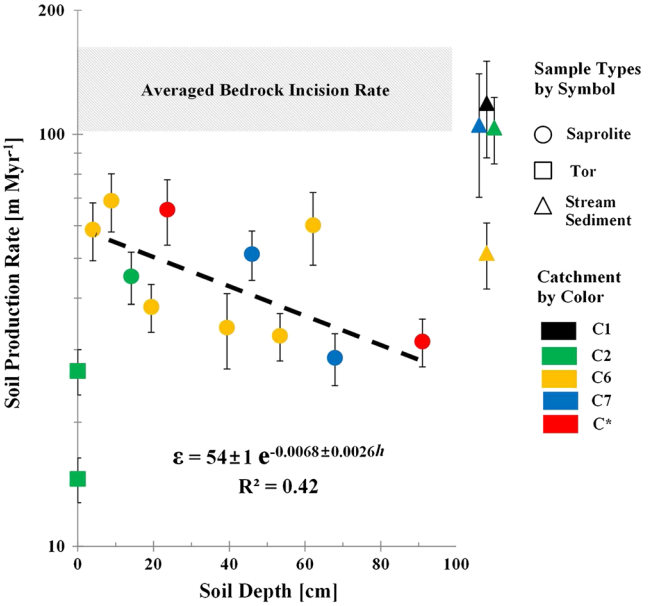

Figure 7. Soil production rate versus soil depth, catchment-wide denudation rates, and averaged bedrock incision rate. Sample types and sub-catchments used for soil production rates are shown in the legend by symbols and colors respectively, as shown in Figure 3. Different error bars come from depth, density and ^{10}Be concentration (Tables I and II). C* is a sub-catchment between sub-catchments C2 and C6 but does not have a measured catchment-wide denudation rate because of limited accessibility to the catchment. The dashed line is the soil production function with the variance weighted regression equation noted. The gray box in the figure shows a range for the averaged bedrock incision rate calculated from the exposure age of strath terraces (Supplementary Figure 3). This figure is available in colour online at wileyonlinelibrary.com/journal/espl

nearly 2 m, the base-level lowering due to the propagation of the knickpoint is thought not to be significant enough to bring drastic change in denudation rate in the study area, because the catchment-wide denudation rate of the sub-catchment C6, which might have already experienced (or been experiencing) knickpoint migration, is not much different from those of sub-catchments (C1, C2, C6, C7) that are located upstream of the knickpoint and therefore have not yet experienced the base-level lowering associated with propagation of the knickpoint. Since several knickpoints similar in size to the above knickpoint are found on the longitudinal profile of the Song River (Figure 1(D)), sudden changes in bedrock incision rate might have occurred repetitively over time.

Controls on catchment-wide denudation

Many studies have explored the relationships between denudation and topographic forms: relief or slope (Summerfield and Hulton, 1994; Binnie *et al.*, 2007; Roering *et al.*, 2007; Ouimet *et al.*, 2009; DiBiase *et al.*, 2010; Portenga *et al.*, 2013), upstream contributing area (Stock and Montgomery, 1999), and curvature (Roering *et al.*, 1999; Hurst *et al.*, 2012). In the case of high-altitude regions characterized by alpine climate, frost cracking beneath the ground surface and orographic precipitation play major roles in transporting surface materials downslope (Anderson, 2002; Kober *et al.*, 2007; Delunel *et al.*, 2010; Anderson *et al.*, 2013). However, our catchment-wide denudation rates do not reveal strong correlations with slope, relief, elevation, and precipitation (Figure 6). Such weak correlations imply that the denudation rates of the Daegwanryeong Plateau are controlled by transport processes not only affected by the topographic features but also driven by the alpine climate.

Conversely, the mean value of the denudation rates (~93 ± 22 m Myr^{-1}) is similar to the averaged bedrock incision rate (~128 ± 27 m Myr^{-1}). Considering downslope transport times for soils on such hillslopes are long (McKean *et al.*, 1993), the values of catchment-wide denudation rates we calculated might be too high due to the potential for additional nuclide production during downslope transport. If this were the case, then the difference between the mean value of denudation rates and the averaged bedrock incision rate would be much smaller. Such a possibility suggests that the denudation rate of the Daegwanryeong Plateau is likely to be controlled by the bedrock incision rate.

Weak depth dependency of soil production rate

To validate our soil production rates and function in terms of the effects from recent land use change from native forest to pasture since the 1970s, we calculated the potential soil production rates and function considering possible soil loss due to the land-use change. First, we added a probable soil thickness, which may have been eroded additionally due to the land use change, to our soil thickness measurement values. The additional eroded soil thickness is estimated to be ~9 mm determined from soil loss data including the Daegwanryeong Plateau (Park *et al.*, 2010). Then, we recalculated soil production rates with the additional soil depths. According to the comparison with the recalculated data, the difference between the

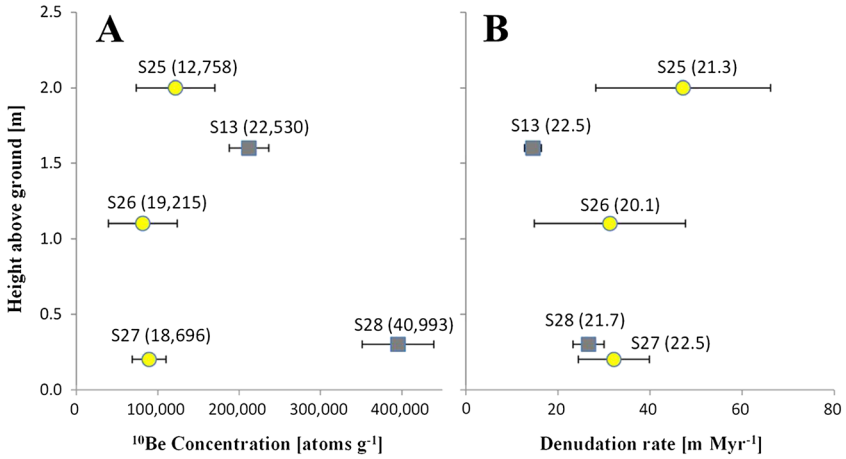

Figure 8. ^{10}Be concentrations and denudation rates of samples from a tor profile (●) and other tor surfaces (□). The values in brackets in (A) and (B) are the effective exposure ages (in years) and mean rebound values measured by Schmidt hammer, respectively. See text for more discussion. This figure is available in colour online at wileyonlinelibrary.com/journal/espl

two data sets is small (0.40 ± 0.20 m Myr^{-1}). Moreover, if we recalculate the soil production function with even ten times the probable eroded soil thickness (i.e. 90 mm thicker soils), the function does not differ from Equation (1). Such an insignificant difference in the soil production rates comes from the high concentrations of cosmogenic nuclides due to the high elevation of the plateau.

The exponentially decreasing pattern of soil production rate with depth that we observed in the study area is consistent with those of previously published global soil production data (Figure 9). One interesting aspect of the pattern of our soil production function is the relatively low value of decay constant in the function (~ -0.007), which is the inverse of e-folding depth, such that the difference in soil production rates between shallow and thick soil thickness is not substantial. Namely, the soil production rate beneath thick soil cover is relatively higher than for previously observed soil production functions, and, therefore, the depth dependency of soil production rates is not as high as those found in other areas.

A recent study (Dixon *et al.*, 2009), which also reported an uncertain depth dependence of soil production rate at a high altitude soil-mantled landscape, suggested possible reasons for the uncertain depth dependency: overland flow erosion occurring as a dominant transport process rather than biotically or freeze-thaw driven hillslope process erosion; soil depths temporarily out of local steady state; and analytical anomalies in the samples. The erosion of the Daegwanryeong Plateau is, however, not dominated by overland flow but by frost creep (Kee, 2002), and therefore the soil production in the study area is also likely to be controlled by the same processes (Heimsath and Jungers, 2013). Moreover, unlike the relationship of Dixon *et al.* (2009)'s data, the depth dependency of soil production rate is weak in our data ($R^2 = 0.42$). Although we cannot exclude any possibility of either the soil depths being out of local steady state or anomalies in the samples, the weak depth dependency may originate from the natural soil production processes.

Although an explicit consideration of the role of bedrock weathering status has not been tightly integrated into soil production mechanisms, the weak dependency of soil production rate on soil thickness may result from the easily breakable bedrock in the study area. Most of our study area is underlain by chemically weathered, deep saprolites that are easily disaggregated by hand. The physical resistance of chemically weathered bedrock to deformation under stress is so small (Begonha and Sequeira Braga, 2002) that the saprolites at the bottom of the soil layer are likely to be easily perturbed by living organisms and frost cracking. Because we found no evidence for bioturbation, such as macro fauna burrowing in the study area, we believe that the highly weathered bedrock coupled with frequent frost action enables the weak dependency of soil production rate on thickness.

To test the effect of frost cracking on the pattern of our soil production data, we calculated frost cracking intensity based on the assumption that segregation ice-lens growth is an efficient frost shattering mechanism (Murton *et al.*, 2006) and that the maximum ice-growth rate is attained within the 'frost-cracking window' (Anderson, 1998). First, we estimated the representative profiles of underground temperature of the study area through time and depth using a one-dimensional heat conduction model given a sinusoidal surface temperature variation (Hales and Roering, 2007) (Figure 10(A)). Then, we calculated the temperature gradient, with which the growth rate of segregation ice varies (Worster and Wettlaufer, 1999), through the depths where the temperature is between -3 and -8 °C (i.e. frost cracking window) (Figure 10(B)). Finally, all temperature gradients were summed up over the course of an annual cycle to quantify the rate of segregation ice growth (Figure 10(C)).

The modeled underground temperature profiles show that frost cracking could occur frequently within the study area. Assuming that the annual sum of the temperature gradient is a proxy for the frost cracking intensity, our data suggest that frost cracking intensity is not highest near the surface but rather at depth (Figure 10(C)). Since the physical strength of the saprolites is low, the saprolites may be more disturbed by the frost cracking than unweathered bedrock. Consequently, the potential strength variation of saprolites with depth may be directly influenced by the variation of frost cracking intensity with depth. This implies that the saprolite at some depth with lower strength due to more intensive frost cracking may be more susceptible to being entrained into the mobile soil (Anderson *et al.*, 2013). If this is the case, then the soil production rate at deep depths (>30 cm) might be higher than it would be in areas not underlain by saprolite (Figure 11). The soil depth at which the frost cracking intensity peaks in our simple simulation could be a basis for a hump-back shaped soil production function rather than the exponentially decreasing function. However, the potential effect of variation of the frost cracking intensity on the soil production processes in the study area does not appear to dominate those of the depth-dependent soil production processes, because the observed weak exponential decline of soil production rates is far from the potential humped soil production curve.

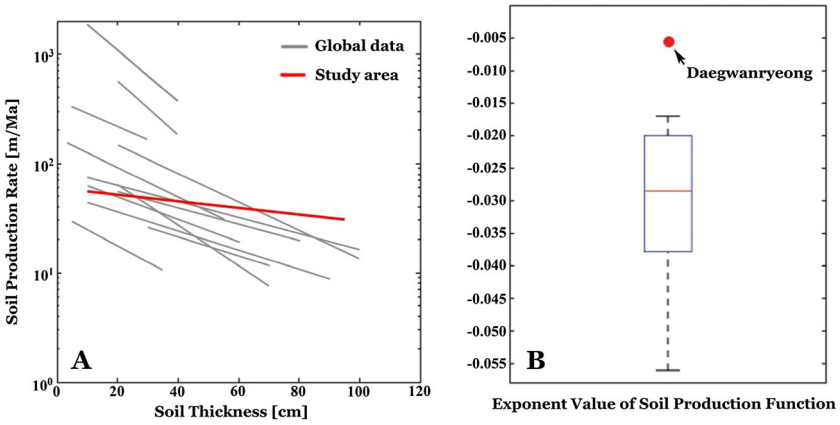

Figure 9. Comparison with global soil production data. (A) Soil production function observed here with worldwide compilation of the previously published soil production functions (Heimsath *et al.*, 1997, 2000, 2001a, 2001b, 2005, 2009, 2012; Dixon *et al.*, 2009; Owen *et al.*, 2011; Larsen *et al.*, 2014). (B) Box plot showing both our exponent value (-0.0068) and the range of the exponent values of the previously published soil production functions (n = 12, mean = -0.0309, minimum = -0.056, maximum = -0.017). This figure is available in colour online at wileyonlinelibrary.com/journal/espl

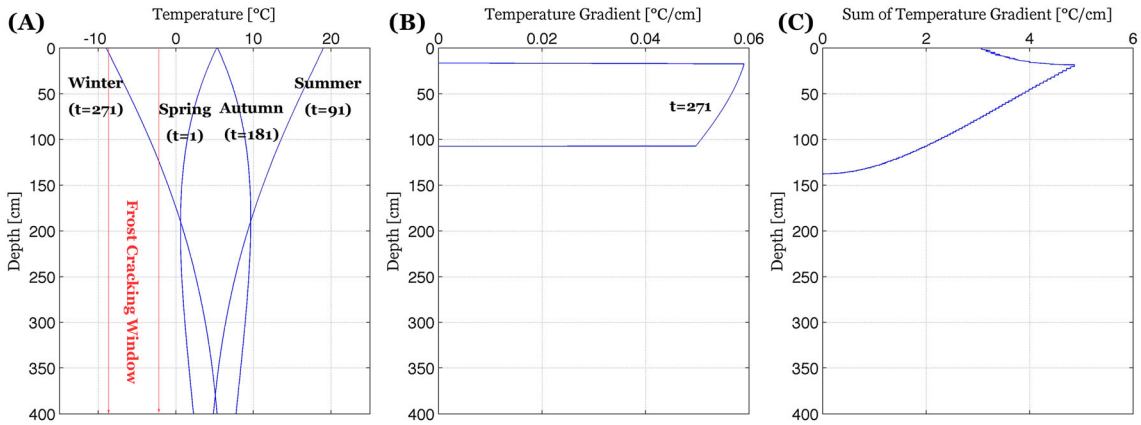

Figure 10. (A) Representative underground temperature profiles of the study area with a mean annual temperature of 5 °C and an annual temperature variation of 14 °C, which are the results of the heat flow model by Hales and Roering (2007), at time steps 1 (spring), 91 (summer), 181 (autumn), and 271 (winter). These temperatures used in this model are calculated using the data from the nearest climate observatory at 772 m (http://www.kma.go.kr) and digital climate model provided by the National Center for Agro Meteorology (http://www.ncam.kr), and the temperature profile is also corrected by the underground temperature data observed in the study area (Lee, 1992). (B) Representative temperature gradient with depth at time step 271 (winter) of the study area. (C) Representative annual sum of temperature gradient with depth of the study area. This figure is available in colour online at wileyonlinelibrary.com/journal/espl

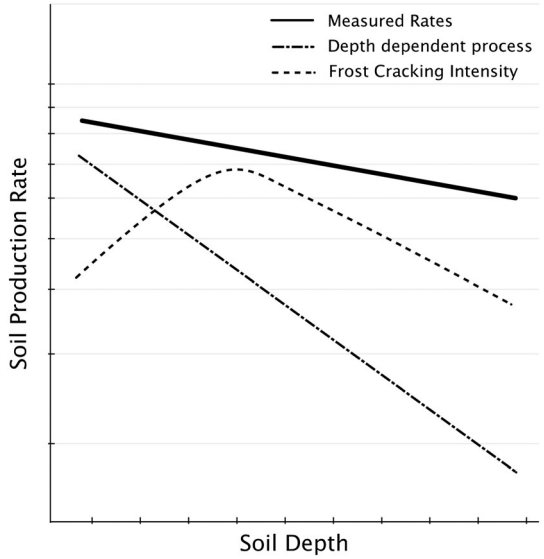

Figure 11. Conceptual model illustrating the potential impact of highly weathered bedrock coupled with frequent frost action on the soil production function in the study area. Dashed line (- · -) represents a typical soil production function by depth dependent soil production mechanisms. Low resistant bedrock in the study area (i.e. chemically weathered saprolite) could reflect well the effects of the intensive frost cracking on soil production (dotted line). Therefore, the coupling of these two processes may lead to a weak depth dependence of soil production rate with depth (solid line).

Development of the Tors

The denudation rates of the samples from the top surfaces of the two lower tors (S13, S28), which are plotted as zero-depth samples shown by squares in Figure 7, reflect unweathered bedrock denudation rather than soil production processes. They are lower than even the lowest soil production rate (S5) that is indicative of the lowest soil surface lowering rate, and thus the tors in the study area are expected to grow continuously once they are exposed. Additional data of the samples taken vertically from the tallest tor in the study area provide an opportunity to reveal a detailed history for tor development, as well as soil lowering around the tor. If a tor has emerged steadily rather than episodically, then nuclide concentrations from the tor profile samples would increase upwards from the ground surface (Heimsath *et al.*, 2001a, 2001b). Given the similar exposure ages (i.e. ^{10}Be concentrations) of all the samples from the tallest tor (Figure 8), the soil-mantled ground surface around the tallest tor is likely, instead, to have been suddenly lowered since the exposure of the tor. Although we cannot exclude any possibility for localized hillslope slump exposing the tor, comparison of the samples from the tallest tor with those from the two lower tors and supplementary field observations do not support this notion.

First, field observations from the top surface of the tallest tor suggest that the tor may have been eroding episodically by block disintegration along a joint plane rather than by steady, grain-by-grain spallation. The tor for profile sampling is the tallest in the local area, and thus its exposure age is expected to exceed those of the other tors. Conversely, its exposure age (S25) is younger than those of other shorter tors (S13, S28) (Figure 8(A)), and also younger than even those of both the middle (S26) and bottom (S27) points of the tallest tor. Moreover, its denudation rate is marginally greater than those of the shorter tors (Figure 8(B)). Considering that the Schmidt hammer rebound value of sample point S25 is similar to those of other sample points (Figure 8(B)), it is unlikely that the difference in calculated denudation rate is related to a difference in the degree of weathering. Given that the tallest tor has a flat, instead of domed, top surface (Figure 4(F)), the top surface of the tor might have been recently eroded by an episode of block disintegration that would yield a lower ^{10}Be concentration and higher denudation rate than would otherwise be the case. Second, the side of the tallest tor might have been eroded by strong winds for some periods of its history. In the study area, trees deflected and tors abraded by strong wind are observed across the ridges of hillslopes (Kee, 1999). Since the middle sampling point (S26) is indented unlike the bottom point (S27) (Figure 4(F)), and faces the west from which most winds blow, the sampled side of the tor also might have been eroded by strong winds during some period (prior to 19 000 years ago) characterized by a cold and arid peri-glacial environment. This accelerated erosion by strong winds could account for the similar ^{10}Be concentrations of S26 and S27 to that of S29.

Although our ^{10}Be data from the tallest tor cannot answer the question of whether the tor emerged or the ground surface has been lowered steadily or not, the combined analysis based on both our ^{10}Be data and field observations indicates that the tors in the study area emerged recently and that growth of the tors may have not been consistent due to intermittent block

disintegration and intensive erosion by strong winds during colder and windier periods in the past. Furthermore, these results also imply that application of cosmogenic nuclides for understanding tor development or soil denudation should be carefully carried out corresponding to field specific conditions.

Transient state of the landscape

Because soil production values equate to a ground surface lowering rate at the point, comparison between soil production and catchment-wide denudation rates enables testing the potential equilibrium state of the landscape. If the catchment-wide denudation rates are equivalent to the soil production rates, the landscape of the Daegwanryeong Plateau would be in morphological equilibrium. We observed, instead, that the mean soil production rate is significantly lower than the mean catchment-wide denudation rate (Figure 7). This suggests that broadly convex hilltops are eroding more slowly than other parts of the study area, because the sampled sites for soil production rate are mostly located at the convex ridge tops of soil-mantled hillslopes.

Although we need more soil production data from other parts of the plateau to fully address the disconnect between point-specific soil production rates and the catchment-wide denudation rates, such a difference could imply that recently accelerated stream incision has not fully propagated to the upper convex part of the hillslope (Hurst *et al.*, 2012) and thus the sub-catchments in the plateau exist in a transient state. This transience could be driven by sudden changes in bedrock incision rates, such as the change supported by our data. Namely, the landscape of the Daegwanryeong Plateau has been denuding constantly in the long-term, but it has been in a transient state triggered by intermittent base-level lowering events in the short-term.

Landscape evolution of the Daegwanryeong plateau

The long-term landscape evolution of the Daegwanryeong Plateau remains poorly constrained. Previous studies (Kim, 1973, 1980) suggest that the currently observed low-relief, hilly landscape is the remnant of an uplifted, paleo erosional surface. According to their interpretation, the initial surface or landscape of the plateau had formed at a paleo sea level before the mid-Miocene at latest, and then had been maintained to date. If this interpretation is true, the denudation rate of the Daegwanryeong Plateau should be extremely low to maintain its initial landscape, and the paleo denudation rate of the initial surface should be preserved. However, although the data that we report here spans only the late Quaternary, they do suggest that the current landscape of the Daegwanryeong Plateau does not reflect the probable initial landscape of a paleo erosional surface and is, therefore, not a paleo surface.

First, comparison of our denudation data with those from other paleo-surfaces shows that the denudation rate of the Daegwanryeong Plateau is not comparatively low (Supplementary Figure 4). The denudation rates based on cosmogenic nuclides from global paleo-surfaces under diverse climates (dry to wet), altitudes (low to high), surface materials (exposed rock to thick weathered profile), and tectonic settings (stable to active) do not exceed ~20 m Myr^{-1}, and are distinctly differentiated from those of the regions around the paleo-surfaces (Vanacker *et al.*, 2007; Walcek and Hoke, 2012). The denudation rates in the Daegwanryeong Plateau are, instead, two to ten times greater than those of other paleo-surfaces. We cannot provide the exact criterion on the range of denudation rate to enable interpretation as a paleo-surface. However, if the averaged denudation rate in the study area (~93 m Myr^{-1}) is thought to have been similar since the time when the Daegwanryeong Plateau might have formed (the mid-Miocene), then at least 1800 m of landscape overlying the current plateau surface would have been eroded. Such a huge amount of erosion would never permit the initial landscape of the Daegwanryeong Plateau to be maintained without substantial modification. Moreover, the transient state of the landscape corresponding to intermittent base-level lowering events in the short term might also make it difficult for the landscape to maintain its initial form.

Second, the exposure ages of the sparsely distributed tors underlain by deep saprolites in the Daegwanryeong Plateau range from 23 to 41 Ka, and their denudation rates are on average 20 m Myr^{-1}. Moreover, the tallest tor is shown to have been recently eroded by overburden block disintegration. These results imply that the tors have developed rapidly since the late Quaternary. Previous work interpreted the tors as fossil landforms that originated from core stones formed by deep weathering under much warmer and humid climate conditions before at least the late Tertiary, and then exhumed by the stripping of overlying saprolites under the colder climate in the Quaternary (Kim, 1980). This interpretation provided another basis for the longevity of the Daegwanryeong Plateau. However, this argument would be compelling only if the eroded amounts of the overlying saprolites were very small and the denudation rates of the tors were extremely low. The combination of substantial soil production since the early Quaternary (~100 m = 50 m Myr^{-1} averaged soil production rate in the study area × 2 Myr) and the relatively rapid tor development suggests strongly that the tor formation does not reflect Tertiary processes.

Third, the averaged bedrock incision rate within the Daegwanryeong Plateau is similar to that of the westerly drainage of the plateau, which does not include any low-relief landscape feature. Previous studies reported the marked discrepancy in denudation rates between paleo-surfaces and their surrounding areas (Vanacker *et al.*, 2007; Walcek and Hoke, 2012). In contrast, the similarity of our bedrock incision rate to that of surrounding areas raises the possibility that the landscape of the plateau has not been controlled by the paleo incision rate that formed the paleo-surface, but by the modern incision rate after the neo-tectonic activity of the Korean Peninsula. Further investigation into the denudation rates of the catchments surrounding the plateau will help confirm this interpretation.

Our cosmogenic interpretation shows that the Daegwanryeong Plateau is not a paleo-surface, and thus its low-relief landscape remains enigmatic. One possible explanation for the low relief could be the deeply weathered saprolites in the plateau. Easily erodible surface materials, especially in a tectonically quiescent region, are likely to lead to a low-relief landscape compared with the high-relief landscape in the surrounding areas of more resistant lithology (Song, 1994). Moreover, the saprolite likely enables easier modification of the probable initial form of the plateau into the current, rounded hillslopes, which are regarded as the final morphology from diffusive hillslope processes regardless of the initial form of the landscape (Fernandes and Dietrich, 1997; Anderson, 2002). Although our data do not resolve the origins of the plateau, they do suggest specific avenues for further research to help resolve what processes generated the low-relief landscape of the Daegwanryeong Plateau.

Conclusion

We applied several cosmogenic nuclide techniques to establish a comprehensive understanding of the landscape development

of a high-altitude, low-relief area (HLA), specifically the Daegwanryeong Plateau of the Korean Peninsula. Our denudation data provide quantitative information on the key geomorphic processes that have acted on the plateau: (1) the base-level lowering rate in the plateau is consistent with the regional tectonics of the western part of the Korean Peninsula; (2) the catchment-wide denudation rates of the plateau are mainly controlled by the bedrock incision rate within the plateau, rather than the surface processes driven by topographic features or alpine climate; (3) the soil production function we observed shows weak depth dependency that may result from highly weathered bedrock coupled with frequent frost actions under the alpine climate; (4) the lower soil production rates than the catchment-wide denudation rates indicate that the landscapes in the plateau are in a transient state; and (5) the tors once regarded as fossil landforms from the Tertiary have developed since the late Quaternary, and thus do not reflect Tertiary processes.

The rapid denudation compared with those of global paleo-surfaces and the reported development processes of the Daegwanryeong Plateau suggest that the plateau cannot have maintained the initial landscape of paleo-surfaces that formed near a paleo sea level and thus is not a paleo-surface. Low relief of the Daegwanryeong Plateau may simply result from easily erodible surface materials over a tectonically quiescent region. Although our data do not clearly resolve the origin of the Daegwanryeong Plateau, they contribute to understanding both the active geomorphic processes and the evolution of an actively eroding upland landscape, as well as calling into question our interpretations of supposed paleo-surfaces around the world. Furthermore, our comprehensive approach adapted to the Daegwanryeong Plateau could be a new standard for investigating other HLAs around the globe.

Acknowledgements—We sincerely thank all the reviewers for their time and efforts. Their valuable comments and suggestions helped improve this article. We also appreciate the approval of the Korean National Park Service to permit sampling in the Daegwanryeong Plateau. The correlation analysis in this study are based on 'High Definition Digital Climate Maps' of the National Center for Agro-Meteorology available through the Ministry of Agriculture, Food and Rural Affairs funding. This work was supported by the National Research Foundation of Korea Grant funded by the Korean Government (NRF-2012S1A5B5A01025420).

References

Abbott L, Silver E, Anderson R, Smith R, Ingle J, Kling S, Sliter W. 1997. Measurement of tectonic surface uplift rate in a young collisional mountain belt. *Nature* **385**: 501–507.

Anderson RS. 1998. Near-surface thermal profiles in alpine bedrock: implications for the frost weathering of rock. *Artic and Alpine Research* **30**: 362–372.

Anderson R. 2002. Modeling the tor-dotted crests, bedrock edges, and parabolic profiles of high alpine surfaces of the Wind River Range, Wyoming. *Geomorphology* **46**: 35–58.

Anderson RS, Anderson SP, Tucker GE. 2013. Rock damage and regolith transport by frost: an example of climate modulation of the geomorphology of the critical zone. *Earth Surface Processes and Landforms* **38**: 299–316.

Babault J, Van Den Driess J, Bonnet S, Castelltort S, Crave A. 2005. Origin of the highly elevated Pyrenean peneplain. *Tectonics* **24**: TC2010. DOI: 10.1029/2004TC001697

Begonha A, Sequeira Braga MA. 2002. Weathering of the Oporto granite: geotechnical and physical properties. *Catena* **49**: 57–76.

Belton DX, Brown RW, Kohn BP, Fink D, Farley KA. 2004. Quantitative resolution of the debate over antiquity of the central Australian landscape: implications for the tectonic and geomorphic stability of cratonic interiors. *Earth and Planetary Science Letters* **219**: 21–34.

Bierman P, Steig E. 1996. Estimating rates of denudation using cosmogenic isotope abundances in sediment. *Annual Review of Earth and Planetary Sciences* **21**: 125–139.

Brown ET, Stallard RF, Larsen MC, Raisbeck GM, Yiou G. 1995. Denudation rates determined from the accumulation of *in situ* produced ^{10}Be in the Luquillo Experimental Forest, Puerto Rico. *Earth and Planetary Science Letters* **129**: 193–202.

Byun J. 2011. Development and application of a numerical landscape evolution model to understand the uplift history of the Korean Peninsula. Unpublished PhD dissertation, Seoul National University (in Korean with English abstract).

Chmeleff J, von Blanckenburg F, Kossert K, Jakob D. 2010. Determination of the ^{10}Be half-life by multicollector ICP-MS and liquid scintillation counting. *Nuclear Instruments and Methods in Physics Research Section B: Beam Interactions with Materials and Atoms* **268**: 192–199.

Clark MK, House MA, Royden LH, Whipple KX, Burchfiel BC, Zhang X, Tang W. 2005. Late cenozoic uplift of southeastern Tibet. *Geology* **33**: 525–528.

Delunel R, van der Beek PA, Carcaillet J, Bourlès DL, Valla PG. 2010. Frost-cracking control on catchment denudation rates: insights from *in situ* produced ^{10}Be concentrations in stream sediments (Ecrins-Pelvoux massif, French Western Alps). *Earth and Planetary Science Letters* **293**: 72–83.

de Sitter LU. 1952. Pliocene uplift of Tertiary mountain chains. *American Journal of Science* **250**: 297–307.

DiBiase RA, Whipple KX, Heimsath AM, Ouimet WB. 2010. Landscape form and millennial erosion rates in the San Gabriel Mountains, CA. *Earth and Planetary Science Letters* **289**: 134–144.

Dixon JL, Heimsath AM, Kast J, Amundson R. 2009. Climate-driven processes of hillslope weathering. *Geology* **37**: 975–978.

Dunai TJ. 2010. *Cosmogenic Nuclides: Principles, Concepts and Applications in the Earth Surface Sciences*. Cambridge University Press: New York.

Editorial board for Samyang Food's thirty year history. 1991. *Samyang Food's thirty year history*. Samyang Foods: Seoul. (in Korean).

Epis RC, Chapin CE. 1975. Geomorphic and tectonic implications of the post-Laramide, late eocene erosion surface in the southern rocky mountains. *Geological Society of America Memoir* **144**: 45–74.

Fernandes NF, Dietrich WE. 1997. Hillslope evolution by diffusive processes: the timescale for equilibrium adjustments. *Water Resources Research* **33**: 1307–1318.

Finnegan NJ, Schumer R, Finnegan S. 2014. A signature of transience in bedrock river incision rates over timescales of 10^4–10^7 years. *Nature* **505**: 391–394.

Gosse JC. Phillips FM. 2001. Terrestrial *in situ* cosmogenic nuclides: theory and application. *Quaternary Science Reviews* **20**: 1475–1560.

Goudie AS. 2006. The Schmidt hammer in geomorphological research. *Progress in Physical Geography* **30**: 703–718.

Granger D, Kirchner J, Finkel R. 1996. Spatially averaged long-term erosion rates measured from *in situ*-produced cosmogenic nuclides in alluvial sediment. *Journal of Geology* **104**: 29–257.

Granger D, Lifton NA, Willenbring JK. 2013. A cosmic trip: 25 years of cosmogenic nuclides in geology. *Geology* **125**: 1379–1402.

Gregory KM, Chase CG. 1994. Tectonic and climatic significance of a late Eocene low-relief, high-level geomorphic surface, Colorado. *Journal of Geophysical Research* **99**: 20141–20160.

Gunnell Y. 1998. The interaction between geological structure and global tectonics in multistoried landscape development: a denudation chronology of the South Indian shield. *Basin Research* **10**: 281–310.

Gunnell Y, Calvet M, Brichau S, Carter A, Aguilar JP, Zeyen H. 2009. Low long-term erosion rates in high-energy mountain belts: Insights from thermo- and bio-chronology in the Eastern Pyrenees. *Earth and Planetary Science Letters* **278**: 208–218.

Hales TC, Roering JJ. 2007. Climatic controls on frost cracking and implications for the evolution of bedrock landscapes. *Journal of Geophysical Research* **112**: F02033. DOI: 10.1029/2006JF000616

Han JW. 2002. Uplift history of the Taebaeksan range in the Daegwallyeong area using fission track analysis. Unpublished MS dissertation, Seoul National University.

Hancock G, Kirwan M. 2007. Summit erosion rates deduced from ^{10}Be: implications for relief production in the central Appalachians. *Geology* **35**: 89–92.

Heimsath AM, Chappell J, Dietrich WE, Nishiizumi K, Finkel RC. 2000. Soil production on a retreating escarpment in southeastern Australia. *Geology* **28**: 787–790.

Heimsath AM, Chappell J, Dietrich W, Nishiizumi K, Finkel R. 2001a. Late Quaternary erosion in southeastern Australia: a field example using cosmogenic nuclides. *Quaternary International* **83–85**: 169–185.

Heimsath AM, DiBiase RA, Whipple KX. 2012. Soil production limits and the transition to bedrock dominated landscapes. *Nature Geosciences* **5**: 210–214.

Heimsath AM, Dietrich W, Nishiizumi K, Finkel R. 1997. The soil production function and landscape equilibrium. *Nature* **388**: 358–361.

Heimsath AM, Fink D, Hancock GR. 2009. The 'humped' soil production function: eroding Arnhem land, Australia. *Earth Surface Processes and Landforms* **34**: 1674–1684.

Heimsath AM, Furbish DJ, Dietrich WE. 2005. The illusion of diffusion: field evidence for depth-dependent sediment transport. *Geology* **33**: 949–952.

Heimsath AM, Jungers MC. 2013. Processes, transport, deposition, and landforms: quantifying creep. In *Treatise on Geomorphology*, Shroder J, Marston R, Stoffel M (eds). Elsevier: Amsterdam; 138–151.

Heimsath AM, William ED, Kunihiko N, Robert CF. 2001b. Stochastic processes of soil production and transport: erosion rates, topographic variation and cosmogenic nuclides in the Oregon Coast Range. *Earth Surface Processes and Landforms* **26**: 531–552.

Hurst MD, Mudd SM, Walcott R, Attal M, Yoo K. 2012. Using hilltop curvature to derive the spatial distribution of erosion rates. *Journal of Geophysical Research* **117**: F02017. DOI: 10.1029/2011JF002057

Jolivet M, Ritz J-F, Vassallo R, Larroque C, Braucher R, Todbileg M, Chauvet A, Sue C, Arnaud N, De Vicente R, Arzhanikova A, Arzhanikov S. 2007. Mongolian summits: an uplifted, flat, old but still preserved erosion surface. *Geology* **35**: 871–874.

Kee K. 1999. Morpho-pedologic milieu in Taegwanllyong Area. PhD thesis (in Korean with English abstract).

Kee K. 2002. Periglacial millieu in Mt. Sowhangbyung area. *Journal of the Geomorphological Association of Korea* **9**: 45–59. (in Korean with English abstract).

Kennan L, Lamb SH, Hoke L. 1997. High-altitude palaeosurfaces in the Bolivian Andes: evidence for late Cenozoic surface uplift. *Geological Society, London, Special Publications* **120**: 307–323.

Kim S. 1973. Geomorphic studies of the erosion surfaces in central Korea. *Seoul University Journal (A)* **21**: 85–115 (in Korean with English abstract).

Kim S. 1980 An introduction to the tectonics and geomorphic evolution in the Korean Peninsula. *The Geographical Journal of Korea* **5**: 1–15 (in Korean).

Kim I. 1992. Origin and tectonic evolution of the East Sea (Sea of Japan) and the Yangsan Fault System: a new synthetic interpretation. *The Journal of Geological Society of Korea* **28**: 84–109 (in Korean with English abstract).

Kim H. 1994. The characteristics of hillslope form through slope profile analysis - the case study of the Song-cheon river basin. *Journal of Geography Education* **32**: 24–39 (in Korean with English abstract).

Kim J, Ko H, Lee S, Lee C, Choi S, Park K. 2001. *Explanatory note of the Gangreung-Sokcho sheet*. Korea Institute of Geoscience and Mineral Resources (in Korean with English abstract).

Kitayama K. 1992. An altitudinal transect study of the vegetation on Mount Kinabalu, Borneo. *Vegetatio* **102**: 149–171.

Kobayashi T. 1931. Relationship between landscape evolution history of the Korean Peninsula and geological history of the Cenozoic era I II III. *Geography Review* **7**: 523–550, 628–648, 708–732 (in Japanese).

Kober F, Ivy-Ochs S, Schlunegger F, Baur H, Kubik PW, Wieler R. 2007. Denudation rates and a topography-driven rainfall threshold in northern Chile: multiple cosmogenic nuclide data and sediment yield budgets. *Geomorphology* **83**: 97–120.

Kohl CP, Nishiizumi K. 1992. Chemical isolation of quartz for measurement of in situ-produced cosmogenic nuclides. *Geochimica et Cosmochimica Acta* **56**: 3583–3587.

Korschinek G, Bergmaier A, Faestermann T, Gerstmann UC, Knie K, Rugel G, Wallner A, Dillmann I, Dollinger G, von Gostomski CL, Kossert K, Maiti M, Poutivtsev M, Remmert A. 2010. A new value for the half-life of ^{10}Be by heavy-ion elastic recoil detection and liquid scintillation counting. *Nuclear Instruments and Methods in Physics Research Section B: Beam Interactions with Materials and Atoms* **268**: 187–191.

Kwon Y. 2006. The spatial distribution and recent trend of frost occurrence days in South Korea. *Journal of Korean Geographical Society* **41**: 361–372 (in Korean with English abstract).

Lal D. 1988. *In situ*-produced cosmogenic isotopes in terrestrial rocks. *Annual Review of Earth and Planetary Sciences* **16**: 355–388.

Lal D. 1991. Cosmic ray labeling of erosion surfaces: in situ nuclide production rates and erosion models. *Earth and Planetary Science Letters* **104**: 424–439.

Larsen IJ, Almond PC, Eger AE, Stone JO, Montgomery DR, Malcolm B. 2014. Rapid soil production and weathering in the Southern Alps, New Zealand. *Science* **343**: 637–640.

Lee SY. 1992. Altitudinal variation of rainfall in mountains near the Daegwanryeong. Conference proceeding of the Korean Geomorphological Association.

Lee GR. 2009. Properties of channel and evolutions of fluvial terraces in Odae River. *Journal of Korean Geographical Society* **44**: 224–239.

McKean JA, Dietrich WE, Finkel RC, Southon JR, Caffee MW. 1993. Quantification of soil production and downslope creep rates from cosmogenic ^{10}Be accumulations on a hillslope profile. *Geology* **21**: 343–346.

Meisler H. 1962. Origin of erosional surfaces in the Lebanon valley, Pennsylvania. *Geological Society of America Bulletin* **73**: 1071–1082.

Min KK, Cho M, Reiners PW. 2008. Exhumation history of the Taebaek Mountain range in Korean Peninsula: implications for Miocene tectonic evolution of east Asia. EOS Trans, AGU, 89(53), Fall Meet. Suppl, Abstract #T53B-1922.

Min K, Cho M, Reiners PW. 2010. Coeval exhumation of Korean peninsula and opening of east Sea revealed from single-grain (U-Th)/He thermochronology. 12th International Conference on Thermochronology.

Molnar P, England P. 1990. Late Cenozoic uplift of mountain ranges and global climate change: Chicken or egg? *Nature* **346**: 29–34.

Munroe JS. 2006. Investigating the spatial distribution of summit flats in the Uinta Mountains of northeastern Utah, USA. *Geomorphology* **75**: 437–449.

Murton JB, Peterson R, Ozouf JC. 2006. Bedrock fracture by ice segregation in cold regions. *Science* **17**: 1127–1129.

Nishiizumi K, Imamura M, Caffee MW, Southon JR, Finkel RC, McAninch J. 2007. Absolute calibration of ^{10}Be AMS standards. *Nuclear Instruments and Methods in Physics Research Section B: Beam Interactions with Materials and Atoms* **258**: 403–413.

Ouimet WB, Whipple KX, Granger DE. 2009. Beyond threshold hillslopes: channel adjustment to base-level fall in tectonically active mountain ranges. *Geology* **37**: 579–582.

Owen JJ, Amundson R, Dietrich WE, Nishiizumi K, Sutter B, Chong G. 2011. The sensitivity of hillslope bedrock erosion to precipitation. *Earth Surface Processes and Landforms* **36**: 117–135.

Park S. 2009. Are there 'High-level planation surfaces' in the Korean Peninsula? *Journal of the Korean Geomorphological Association* **16**: 91–110 (in Korean with English abstract).

Park BK, Kim SW. 1971. Recent tectonism in the Korean Peninsula and sea floor spreading. *Journal of Korean Institution of Mining Geology* **4**: 39–43.

Park CW, Sonn YK, Zhang YS, Hong SY, Hyun BK, Song KC, Ha SK, Moon YH. 2010. Soil erosion risk assessment in the upper Han River basin using spatial soil erosion map. *Korean Journal of Soil Science and Fertilizer* **43**: 828–836 (in Korean with English abstract).

Pillans B. 2007. Pre-quaternary landscape inheritance in Australia. *Journal of Quaternary Science* **22**: 439–447.

Portenga EW, Bierman PR. 2011. Understanding Earth's eroding surface with ^{10}Be. *Geological Society of America Today* **21**: 4–10.

Portenga EW, Bierman PR, Rizzo DM, Rood DH. 2013. Low rates of bedrock outcrop erosion in the central Appalachian Mountains inferred from *in situ* ^{10}Be. *Geological Society of America Bulletin* **125**: 201–215.

Reuter JM. 2005. Erosion rates and patterns inferred from cosmogenic 10Be in the Susquehanna River Basin. MS thesis, University of Vermont.

Roering JJ, Kirchner JW, Dietrich WE. 1999. Evidence for nonlinear, diffusive sediment transport on hillslopes and implications for landscape morphology. *Water Resources Research* **35**: 853–870.

Roering JJ, Perron JT, Kirchner JW. 2007. Functional relationships between denudation and hillslope form and relief. *Earth and Planetary Science Letters* **264**: 245–258.

Scott GR. 1975. Cenozoic surfaces and deposits in the southern Rocky Mountains. *Geological Society of America Memoirs* **144**: 227–248.

Small EE, Anderson RS. 1998. Pleistocene relief production in Laramide mountain ranges, western United States. *Geology* **26**: 123–126.

Small EE, Anderson RS, Hancock GS. 1999. Estimates of the rate of regolith production using ^{10}Be and ^{26}Al from an alpine hillslope. *Geomorphology* **27**: 131–150.

Small EE, Anderson RS, Repka JL, Finkel R. 1997. Erosion rates of alpine bedrock summit surfaces deduced from *in situ* ^{10}Be and ^{26}Al. *Earth and Planetary Science Letter* **150**: 413–425.

Smith RB. 1979. The influence of mountains on the atmosphere. *Advances in Geophysics* **21**: 87–233.

Song U. 1994. Geomorphic development of incised meander in the Songchŏn. *Geographical Discussion* **14**: 40–55 (in Korean with English Abstract).

Stock JD, Montgomery DR. 1999. Geologic constraints on bedrock river incision using the stream power law. *Journal of Geophysical Research, B: Solid Earth* **104**: 4983–4993.

Stone JO. 2000. Air pressure and cosmogenic isotope production. *Journal of Geophysical Research* **105**: 23753–23759.

Strobl M, Hetzel R, Niedermann S, Ding L, Zhang L. 2012. Landscape evolution of a bedrock peneplain on the southern Tibetan Plateau revealed by *in situ*-produced cosmogenic ^{10}Be and ^{21}Ne. *Geomorphology* **153–154**: 192–204.

Sugai T, Ohmori H. 1999. A model of relief forming by tectonic uplift and valley incision in orogenesis. *Basin Research* **11**: 43–57.

Summerfield MA, Hulton NJ. 1994. Natural controls of fluvial denudation rates in major world drainage basins. *Journal of Geophysical Research, Solid Earth* **99**: 13871–13883.

Trodick CD. 2011. *In situ* and meteoric ^{10}Be concentrations of fluvial sediment collected from the Potomac River Basin. MS thesis, University of Vermont.

Twidale CR, Campbell EM, 1995. Pre-quaternary landforms in the low latitude context: the example of Australia. *Geomorphology* **12**: 17–35.

Vanacker V, von Blanckenburg F, Hewawasam T, Kubik PW. 2007. Constraining landscape development of the Sri Lankan escarpment with cosmogenic nuclides in river sediment. *Earth Surface Processes and Landforms* **253**: 402–414.

van der Beek P, Van Melle J, Guillot S, Pecher A, Reiners PW, Nicolescu S, Latif M. 2009. Eocene Tibetan plateau remnants preserved in the northwest Himalaya. *Nature Geoscience* **2**: 364–368.

von Blanckenburg F, Hewawasam T, Kubik PW. 2004. Cosmogenic nuclide evidence for low weathering and denudation in the wet, tropical highlands of Sri Lanka. *Journal of Geophysical Research, Earth Surface* **109**: F03008. DOI: 10.1029/2003JF000049

Walcek AA, Hoke GD. 2012. Surface uplift and erosion of the southernmost Argentine Precordillera. *Geomorphology* **153–154**: 156–168.

Worster MG, Wettlaufer JS. 1999. The fluid mechanics of premelted liquid films. In *Fluid Dynamics at Interfaces*, Shyy W, Narayanan R (eds). Cambridge University Press: New York; 339–351.

Yoo K, Mudd SM. 2008. Toward process-based modeling of geochemical soil formation across diverse landforms: a new mathematical framework. *Geoderma* **146**: 248–260.

Yoon SO, Hwang S, Lee GR. 2007. Geomorphic evolution of fluvial terraces at Yeongdong · Yeongseo streams in Gangwon Province, Korea. *Journal of Korean Geographical Society* **42**: 388–404.

Supporting Information

Additional supporting information may be found in the online version of this article at the publisher's website.